CrossMark

J. Fluid Mech. (2017), *vol.* 825, *pp.* 651–676. © Cambridge University Press 2017
doi:10.1017/jfm.2017.399

A one-dimensional model for tidal array design based on three-scale dynamics

Vikrant Gupta[1,2,†] **and Anna M. Young**[2]

[1]Department of Mechanics and Aerospace Engineering, Southern University of Science and Technology, Shenzhen, 518055, China

[2]Whittle Laboratory, Department of Engineering, University of Cambridge, Cambridge, CB3 0DY, UK

(Received 20 September 2016; revised 13 May 2017; accepted 31 May 2017; first published online 21 July 2017)

In order to make the extraction of tidal current energy economically viable, the power production per turbine must be optimised in each tidal array. Furthermore, the impact of power extraction on the marine flow environment must be understood. These two aims mean that designers must be able to model different configurations of a tidal array in order to create the most efficient, least invasive arrangement. In this paper, an analytical model is developed for array design in idealised rectangular tidal channels with idealised turbines. The model includes the effects of (i) local blockage, (ii) surface deformation and (iii) added drag due to the installation of the array. While these effects have been accounted for individually in past work, the model presented here is the first to include all three such that the interaction between different effects can be understood. Results are presented for optimal local blockage and turbine resistance as functions of inherent channel drag coefficient, channel length and Froude number at various global blockage values. It will be shown that it is necessary to model the effects of local blockage and added drag simultaneously in order to obtain the design parameters of a tidal array (global blockage, local blockage and turbine resistance), which will maximise the power extraction per turbine. Neglecting either effect will lead to an array design with lower power extraction than the optimum, the addition of unnecessary extra turbines and higher lost power from the array.

Key words: coastal engineering, geophysical and geological flows, hydraulics

1. Introduction

Tidal current energy could emerge as a significant source of energy, particularly in coastal regions with narrow channels and fast currents. The biggest advantage of tidal energy over other renewable energy sources is its predictability and regularity. This is because it is governed by the motion of the sun and moon relative to the Earth, which are regular and indefinitely predictable. Commercially successful extraction of tidal energy, however, requires the power extraction per device to be optimised in order to reduce costs. This means that the total area occupied by an array of turbines, their

† Email address for correspondence: vik.gupta@cantab.net

https://doi.org/10.1017/jfm.2017.399 Published online by Cambridge University Press

arrangement within the array and the drag imposed by the devices on the flow must all be optimised. From an environmental perspective, it is also important to understand the effect of tidal array on the overall channel flow, in order to assess the impact on sediment transport and the local marine ecosystem. The work presented here mainly deals with the challenge of designing tidal arrays for optimal power extraction. It also includes the effect of the installation of a tidal array on the flow velocity at the channel inlet, which is a first step towards determining the environmental impact.

The theoretical limit on the power extracted by an isolated turbine in a large channel has been shown to be 16/27 of the total upstream energy flux through the swept area of the turbine (Lanchester 1915; Betz 1920). This theoretical limit is reached when the turbine is tuned such that flow velocity at the device location is 2/3 of the upstream velocity. In narrow channels, however, this limit can be exceeded. This is because the confining influence of the channel boundaries increases the pressure drop across the turbines, and thus allows more power to be generated (Garrett & Cummins 2007). A simple analytical model developed by Garrett & Cummins (2007) shows that as the turbines occupy a higher proportion of the channel area, the power extraction per turbine can be increased by tuning the turbines such that they have a higher resistance. This means that power extraction per turbine is maximised when the flow is slowed down by a factor of more than 2/3 of the upstream velocity.

The model of Garrett & Cummins (2007), however, ignores the fact that turbines add to the total drag of the channel. They have, therefore, neglected the reduction in the upstream channel flow velocity caused by the additional drag from the turbines. Garrett & Cummins (2005) and Bryden & Couch (2007) have designed simple analytical models to account for this additional drag from the turbines in order to obtain estimates for the maximum power available for extraction. Vennell (2010) developed another analytical model that combines the two models of Garrett & Cummins (2005, 2007) to find the optimal flow blockage by the turbines and their tuning for extracting the maximum fraction of the available power in a given channel. Vennell (2011) then extended his model for tuning the turbines when they are arranged in several rows downstream of each other.

One effect that is not explored in any of the above models is the effect of local blockage on the power extracted by a tidal array. The models of Vennell (2010, 2011) consider the effect of the gap between turbines, but the turbines must be uniformly arranged across the whole channel width (as opposed to a 'partial fence' arrangement where only a fraction of the channel is occupied by the array). Their models also do not consider the effect of the proximity of one turbine on the performance of neighbouring devices (i.e. the local blockage effect). This local blockage effect was first modelled by Nishino & Willden (2012*b*). They developed a quasi-two-scale model, including both the device and the array scale, and used it to explore the efficiency of a long array with infinitely many turbines in a channel. They showed that, for a wide channel (where turbines occupy only a small fraction of the total area), the fraction of available power extracted by each turbine can be increased from the Lanchester–Betz limit of 0.593 (or 16/27) to 0.798 by optimising the local blockage. Nishino & Willden (2013) then extended their model for a finite number of devices and found similar conclusions. Draper & Nishino (2013) have further extended the model to optimise the power extraction per turbine when the devices are arranged in multiple rows, while Vogel, Houlsby & Willden (2016) have included surface deformation effects in their model.

Another model for optimising power extraction which is of particular note here is that of Funke, Farrell & Piggott (2014). They modelled turbines as areas of increased

https://doi.org/10.1017/jfm.2017.399 Published online by Cambridge University Press

bottom friction, solved the shallow water equations for the whole channel (as in Divett, Vennell & Stevens 2011), and optimised the arrangement of the turbines using an adjoint-based method. As pointed out in Adcock, Draper & Nishino (2015), the drawback of Funke *et al.*'s (2014) work is that they fixed the turbines' bottom friction based on the optimal value calculated for a single turbine in isolation, instead of calculating the optimal value based on the actual array arrangement.

In principle, the adjoint-based approach could be extended to include optimal tuning of the turbines based on a specific array arrangement and many more practical constraints. Such a formulation, however, is a long way off (Vennell *et al.* 2015). This is because we have neither the physical understanding required to model many of the relevant effects, nor the computational resources to simulate them. Further to this, the results of Funke *et al.*'s (2014) work are site specific and therefore cannot be used for drawing general conclusions.

In summary, apart from the models of Nishino & Willden (2012*b*, 2013), the models developed to date have not explored the effect of local blockage on the power extraction per turbine. The models of Nishino & Willden (2012*b*, 2013), however, do not account for the effect of added drag due to the installation of a tidal array. Further to this, very few models include the effect of surface deformation. The deformation of the free surface in a channel is proportional to the Froude number and, therefore, is higher in shallow water channels (Whelan, Graham & Peiró 2009; Draper *et al.* 2010; Vogel *et al.* 2016).

The purpose of this paper is to develop an analytical model that includes all three of the effects mentioned above. Firstly, the effect of local blockage is included based on the model given by Nishino & Willden (2013). Secondly, the effect of added drag due to the installation of a tidal array is included based on the model given by Bryden & Couch (2007). Thirdly, the effect of surface deformation is included based on the model given by Whelan *et al.* (2009). To the best of our knowledge, there is no paper in the literature that has yet combined the above three effects in a single analytical model. The model will be used to explore how these three effects together influence the design of tidal array for maximum power generation per turbine, and how treating the effects independently can lead to suboptimal design decisions.

This paper is divided into five sections. Section 2 presents the model derivation. Section 3 presents the results obtained for the optimal resistance of turbines, local blockage and total channel blockage to achieve maximum power extraction per turbine as functions of different channel parameters. Section 4 presents a discussion of the results, a comparison with results from other models in the literature and proposes further improvements to the model. Section 5 concludes the paper.

2. Model description

We consider a simple channel of length L_c with a flat bottom and constant width W_c, as shown in the schematic in figure 1. Tidal head is the only driving force considered, as in Bryden & Couch (2007), and is given as the difference between the water column heights at the channel inlet and outlet ($\Delta h = h_1 - h_5$). It is assumed that the tidal head is unaffected by the presence of turbines in the channel. The upstream channel flow velocity is assumed to be uniform in the vertical direction, and is given by U_1 when no turbines are present. The Froude number of the flow is defined as $Fr = U_1/\sqrt{gh_1}$, where g is acceleration due to gravity. We only consider the quasi-steady case, i.e. time variation of the tidal head is not modelled. Furthermore, we assume that on both sides of the channel (before the inlet and after the outlet) there are large basins of water.

https://doi.org/10.1017/jfm.2017.399 Published online by Cambridge University Press

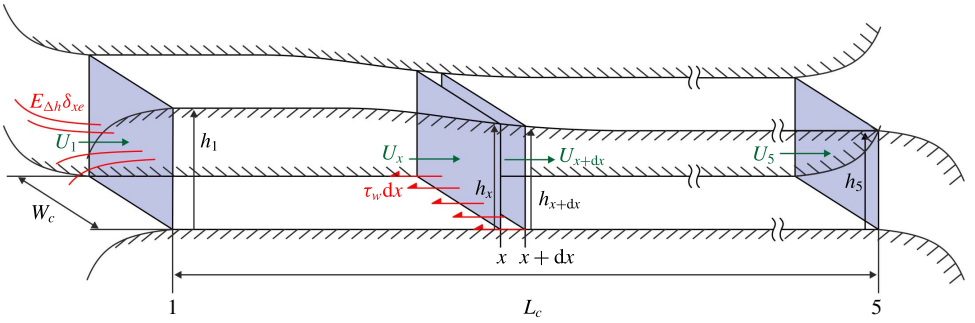


FIGURE 1. (Colour online) A three-dimensional view of the whole channel showing key parameters. The tidal head ($\Delta h = h_1 - h_5$) is assumed to be the only driving term in the channel.

The turbines are modelled as actuator discs, each with diameter L_d and area A_d, and are placed with intra-turbine spacing L_a as shown in figure 2(*a*). They are tuned by adjusting the local induction factor '*a*' (defined in (2.31)), which is a measure of the flow resistance of each turbine. The fraction of the channel inlet area occupied by the turbines is called the global blockage ($B_g = nA_d/W_c h_1$), where n is the number of turbines in the array. The fraction of the channel inlet area occupied by the whole array is called the array blockage ($B_a = nL_aL_d/W_c h_1$). The fraction of each turbine's local flow passage area that is occupied by the turbine is called the local blockage ($B_l = A_d/L_aL_d = B_g/B_a$).

The power extracted per turbine (P_D) is non-dimensionalised by the kinetic energy that would pass through the area occupied by each turbine if the turbines were not present ($(1/2)\rho U_1^3 A_d$). The fraction of this available power extracted per turbine is called the global power coefficient and is given as:

$$C_{PG} = \frac{P_D}{\frac{1}{2}\rho U_1^3 A_d} = \frac{nP_D}{\frac{1}{2}\rho U_1^3 nA_d}. \tag{2.1}$$

An analytical model for a tidal array in the channel described above is obtained by conserving mass, momentum and energy in the axial direction at the channel, array and device scales. In order to close the model, additional equations are obtained from empirical correlations. The hydrostatic approximation, i.e. that the pressure at any point can be expressed in terms of the water column height above that point plus the atmospheric pressure (p_a), is used for obtaining the local pressure at different points in the domain. This approximation is valid as long as there is no significant flow in the vertical direction.

2.1. *Channel-scale conservation equations*

In the absence of turbines, the axial velocity profile is assumed to be uniform in the vertical and cross-span directions. The mass and momentum conservation equations across the small axial element of length dx shown in figure 1, which must be satisfied under all conditions, are:

$$W_c h(x) U(x) = W_c h(x+\mathrm{d}x) U(x+\mathrm{d}x) \implies h(x)\frac{\mathrm{d}U}{\mathrm{d}x} = -U(x)\frac{\mathrm{d}h}{\mathrm{d}x}, \tag{2.2}$$

https://doi.org/10.1017/jfm.2017.399 Published online by Cambridge University Press

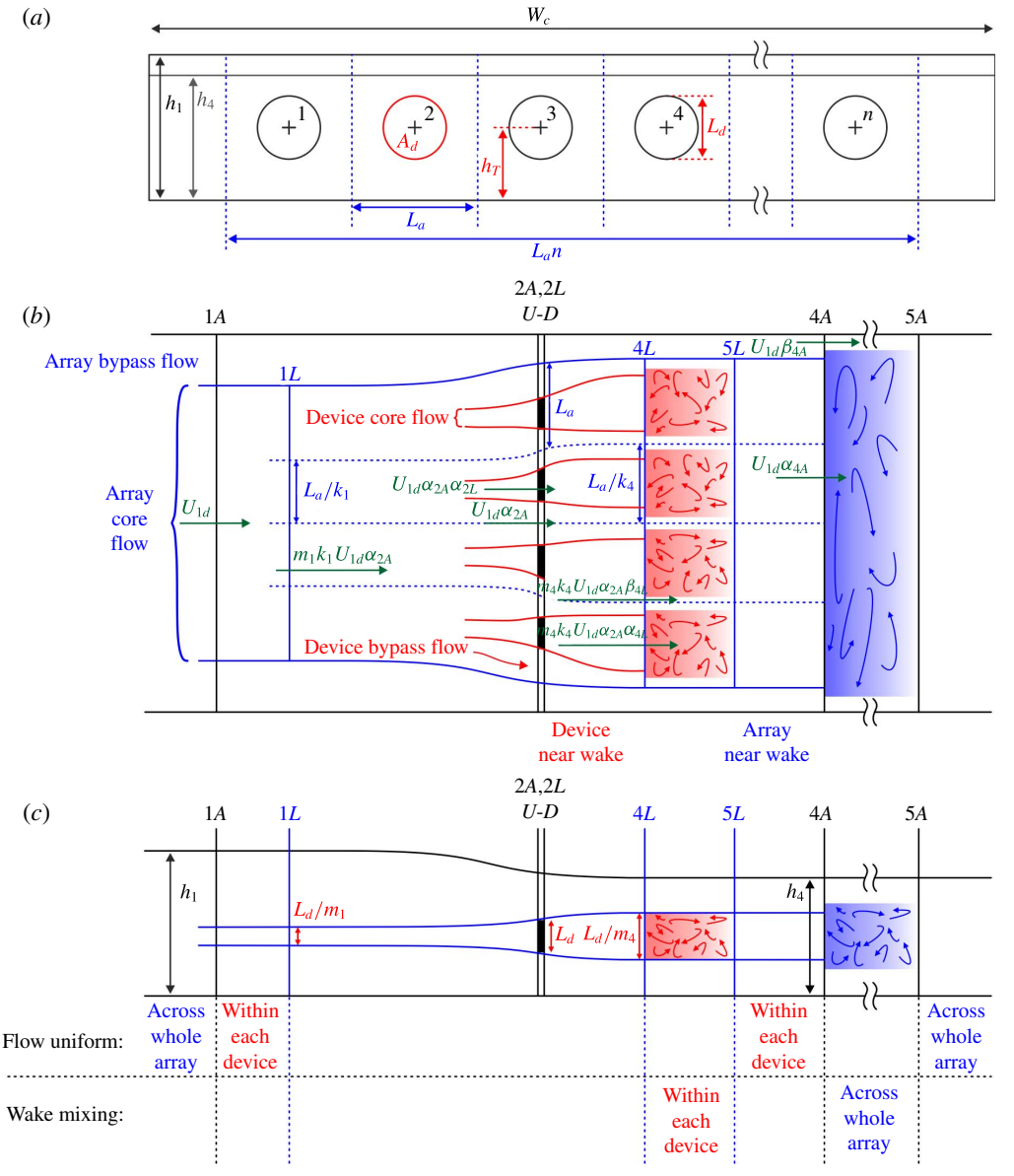


FIGURE 2. (Colour online) The (*a*) front, (*b*) top and (*c*) side views of the tidal array with velocity and length scales shown at key locations. (*a*) Shows that n equi-spaced turbines are arranged in the centre of the channel. (*b*) Shows the array-scale and device-scale core and bypass flows. (*c*) Shows the free surface deformation along the channel.

$$W_c \int_0^{h(x)} [p_a + \rho g(h(x) - y)]\,\mathrm{d}y - W_c \int_0^{h(x+\mathrm{d}x)} [p_a + \rho g(h(x+\mathrm{d}x) - y)]\,\mathrm{d}y$$
$$- W_c p_a(h(x) - h(x+\mathrm{d}x)) - W_c E_{\Delta h}\delta_{xe}\,\mathrm{d}x - W_c \tau_w\,\mathrm{d}x$$
$$= W_c \rho U(x+\mathrm{d}x)^2 h(x+\mathrm{d}x) - W_c \rho U(x)^2 h(x). \tag{2.3}$$

https://doi.org/10.1017/jfm.2017.399 Published online by Cambridge University Press

In the momentum equation, the first three terms are the pressure force terms, $E_{\Delta h}\delta_{xe}$ is the kinetic energy loss term, τ_w is the seabed friction force per unit area and the two terms on the right-hand side are the inertial terms. The kinetic energy loss term ($E_{\Delta h}\delta_{xe}$) and seabed friction (τ_w) are also included in the models given by Garrett & Cummins (2005) and Bryden & Couch (2007) and together they make up the inherent channel drag.

To understand the origin of the kinetic energy loss term, consider the fact that flow enters the channel from a very large basin. It, therefore, has a very small velocity before the inlet. The flow then gains kinetic energy, which is proportional to the square of the channel flow velocity at inlet (U_1). This gain, which is given as $W_c \int_{x_1}^{x_5} E_{\Delta h}\delta_{xe}\,\mathrm{d}x \approx W_c(h_1/2)\rho U_1^2$, must come at the cost of tidal head. Here, the delta function, δ_{xe}, signifies that we account for this term at the channel exit (location 5).

The seabed friction term is commonly taken to be proportional to the square of the flow velocity as $\tau_w = \rho f_1 U(x)^2$, where f_1 is a non-dimensional friction coefficient which is assumed to be constant throughout the channel. The channel modelled here has a constant width and the tidal head drop (Δh) is usually small. Consequently, $U(x)$ does not change much throughout the channel (see (2.3)). So we further simplify the seabed friction to $\tau_w = \rho f_1 U_1^2$.

The models for the two terms of the inherent channel drag are inserted into (2.3) along with (2.2). The resulting equation is then integrated to give a relationship between the undisturbed channel flow velocity (U_1), the tidal head term (Δh) and the drag terms ($f = f_1 L_c + h_1/2$):

$$U_1^2 = \frac{g\Delta h \dfrac{h_1 + h_5}{2}}{\dfrac{h_1}{h_5}\Delta h + f} \implies Fr^2 = \frac{U_1^2}{g h_1} = \frac{\Delta H(1 + H_5)}{C_f}, \tag{2.4}$$

where $C_f = 2[\Delta h/h_5 + f/h_1]$ is the inherent channel drag coefficient and $\Delta H = \Delta h/h_1$ and $H_5 = h_5/h_1$ are the non-dimensional tidal head drop and channel outlet water column height, respectively.

In the presence of a turbine array at one location (say x_T) in the channel, the momentum equation (2.3) is modified such that the thrust imparted by turbines (T_A) is added to the equation as shown by the bold term below:

$$\begin{aligned} W_c \int_0^{h(x)} [p_a + \rho g(h(x) - y)]\,\mathrm{d}y - W_c \int_0^{h(x+\mathrm{d}x)} [p_a + \rho g(h(x+\mathrm{d}x) - y)]\,\mathrm{d}y \\ - W_c p_a(h(x) - h(x+\mathrm{d}x)) - W_c E_{\Delta h}\delta_{xe}\,\mathrm{d}x - W_c \tau_w\,\mathrm{d}x - \boldsymbol{T_A}\delta(\boldsymbol{x} - \boldsymbol{x_T})\,\mathbf{d}\boldsymbol{x} \\ = W_c \rho U(x+\mathrm{d}x)^2 h(x+\mathrm{d}x) - W_c \rho U(x)^2 h(x). \end{aligned} \tag{2.5}$$

The cross-stream variation in the axial flow velocity caused by the array will affect the friction term in the channel $W_c\tau_w\,\mathrm{d}x$. This effect is ignored here for now, but it will be considered in § 2.3, after the array-scale dynamics is introduced. Integrating this modified momentum equation along the length of the channel gives:

$$U_{1nd}^2 = \frac{U_{1d}^2}{U_1^2} = 1 - \frac{T_A}{\frac{1}{2}\rho U_1^2 n A_d} \frac{n A_d}{W_c h_1} \frac{1}{C_f}, \tag{2.6}$$

where U_{1d} is the reduced upstream channel flow velocity and U_{1nd} is its non-dimensional form. The term $T_A/((\rho U_1^2 n A_d)/2)$ is a non-dimensional form of the

https://doi.org/10.1017/jfm.2017.399 Published online by Cambridge University Press

thrust imparted by the turbines and will be referred to as the global thrust coefficient (C_{TG}). Equation (2.6) can then be rewritten as:

$$U_{1nd}^2 = 1 - C_{TG}B_g/C_f. \tag{2.7}$$

This equation shows that the channel flow velocity at the inlet reduces as the thrust imparted by the turbines, C_{TG}, increases. The channel-scale conservation equation (2.7) is our first model equation and contains two unknown variables: U_{1nd} and C_{TG}.

2.1.1. *Estimation of* C_f

The inherent channel drag coefficient (C_f) is a channel parameter which governs the effect of added drag from the turbines. In our model, we vary C_f continuously, but here we give a brief discussion of its physical meaning and of its magnitude in typical marine flows. By assuming that the non-dimensional tidal head drop is small ($\Delta H \ll 1$ – this will be true even in shallow channels), the inherent channel drag coefficient is approximated as:

$$C_f = 2\frac{\Delta H}{H_5} + 2\frac{f_1 L_c + h_1/2}{h_1} \approx 1 + 2\frac{f_1 L_c}{h_1}, \tag{2.8}$$

where f_1 depends up on the roughness of the seabed. This estimation of C_f is similar to that of Bryden & Couch (2007), who use a different friction model. They give the coefficient as $C_f = 1 + 2gn_m^2 L_c/R_d^{(4/3)}$, where R_d is the hydraulic radius of the channel and n_m is the Manning seabed friction coefficient. For the channel considered in Bryden & Couch (2007) (where $L_c = 4000$ m, $W_c = 500$ m, $h_1 = 40$ m and $n_m = 0.025$ sm$^{-1/3}$), the value of C_f is approximately 1.44 (or $1/C_f \approx 0.70$).

Equation (2.7) shows that small values of C_f are desirable, because smaller C_f means larger U_1 for a given ΔH and therefore greater available kinetic energy for a given tidal head. For channels with small C_f, the drag added by the turbines is comparable to the inherent channel drag. This implies that the added drag reduces the channel flow velocity at inlet, i.e. $U_{1nd} < 1$. For those channels with large C_f, the drag added by the turbines is negligible compared to the inherent channel drag. This implies that the added drag has no effect on the upstream channel flow velocity, i.e. $U_{1nd} \approx 1$.

2.2. *Array-scale conservation equations*

Figure 2 shows the (*a*) front, (*b*) top and (*c*) side views of the turbine array. The front view shows that n turbines are arranged symmetrically in the centre of the channel. They are regularly spaced with distance L_a between each other, and each turbine is represented as an actuator disc of diameter L_d (area $A_d = \pi L_d^2/4$). The height of the centre of turbines from the bottom of the channel is h_T, but this term will not appear in the final equations because the upstream velocity profile is assumed to be uniform in the vertical direction. The array inlet and outlet are marked as 1*A* and 5*A*, respectively. We assume that the tidal array is close to the channel inlet such that axial locations 1 in figure 1 and 1*A* in figure 2 coincide. We also assume that the channel is long enough that location 5*A* is upstream of location 5, which means that all the wake mixing behind the array is completed before the channel outlet.

The flow that passes through each turbine is called the device-scale core flow and the flow that passes between the turbines is called the device-scale bypass flow. Similarly, the flow that passes through the array is called the array-scale core flow

https://doi.org/10.1017/jfm.2017.399 Published online by Cambridge University Press

(this flow includes the device-scale core and bypass flows) and the flow that passes between the array and the channel boundaries is called the array-scale bypass flow. The wake mixing regions between $4L$ and $5L$ (device-scale far-wake mixing) and between $4A$ and $5A$ (array-scale far-wake mixing) are shaded in the figure. It is assumed in the model that wake mixing is limited to the shaded regions and that the device-scale and array-scale wake mixing processes happen in separate regions. In reality, however, much of the array-scale wake mixing in the vertical direction is likely to happen between $4L$ and $5L$ (array-scale near-wake region) as opposed to between $4A$ and $5A$. These assumptions, of separate regions of wake mixing for the device and array scales and of the absence of wake mixing in the near-wake region, are limitations of the present model and their implications are discussed in § 4.

At $1A$, both the velocity (U_{1nd}) and channel height (h_1) are uniform across the whole channel width. The locations immediately upstream and downstream of the turbines are marked as U and D, respectively. Neither the velocity nor the channel height are uniform at these locations. The average values of the array-scale dynamical variables between U and D are denoted by the subscript $2A$. The location downstream of turbines where the channel height (h_4) is uniform across the channel width but the flow velocity is still varying is marked as $4A$. The location far downstream where the channel height (h_5) and flow velocity are both uniform is marked as $5A$.

At first, we neglect seabed friction at the array scale and derive the conservation equations. Mass conservation between $1A$ and $4A$ gives:

$$\begin{aligned} U_{1d}h_1W_c \;&=\; U_{1d}\beta_{4A}(h_4W_c - A_{4Ac}) + U_{1d}\alpha_{4A}A_{4Ac} \\ &\Longrightarrow\; 1 = H_4\beta_{4A} + \alpha_{2A}B_a\left(1 - \frac{\beta_{4A}}{\alpha_{4A}}\right), \end{aligned} \tag{2.9}$$

where α_{2A} is the ratio of the core flow velocity at $2A$ to the upstream flow velocity at $1A$, α_{4A} and β_{4A} are the ratios of the core and bypass flow velocities, respectively, at $4A$ to the upstream flow velocity at $1A$. Finally, $A_{4Ac} = nL_aL_d(\alpha_{2A}/\alpha_{4A})$ is the array core flow area at $4A$, and $H_4 = h_4/h_1$.

Considering energy conservation in the array core flow region between $1A$ and $4A$ gives:

$$\begin{aligned} &\frac{1}{2}\rho U_{1d}^3\alpha_{4A}^3A_{4Ac} + U_{1d}\alpha_{4A}\frac{A_{4Ac}}{L_{d4}}\int_{h_T-L_{d4}/2}^{h_T+L_{d4}/2}[p_a + \rho g(h_4 - y)]\,\mathrm{d}y + P_A \\ &\quad= \frac{1}{2}\rho U_{1d}^3A_{1Ac} + U_{1d}\frac{A_{1Ac}}{L_{d1}}\int_{h_T-L_{d1}/2}^{h_T+L_{d1}/2}[p_a + \rho g(h_1 - y)]\,\mathrm{d}y \\ &\quad\Longrightarrow\; U_{1nd}^2(1 - \alpha_{4A}^2) + \frac{2}{Fr^2}(1 - H_4) = B_lC_{TG}, \end{aligned} \tag{2.10}$$

where $A_{1Ac} = nL_aL_d\alpha_{2A}$ is the array core flow area at $1A$, L_{d1} and L_{d4} are the vertical extents of the array core flow regions at $1A$ and $4A$, respectively, and P_A is the power extracted from the flow by the array of turbines (given by $T_AU_{1d}\alpha_{2A}$). Note that P_A is the sum of the useful power extracted by the turbines ($nP_D = T_AU_{1d}\alpha_{2A}\alpha_{2L}$, see § 2.4) and the power dissipated in all the wake mixing regions between $4L$ and $5L$.

Energy conservation for the bypass flow can be satisfied by using Bernoulli's equation, which gives:

$$1 - H_4 = \frac{Fr^2}{2}U_{1nd}^2(\beta_{4A}^2 - 1). \tag{2.11}$$

https://doi.org/10.1017/jfm.2017.399 Published online by Cambridge University Press

The momentum conservation equation for the array-scale flow between 1A and 4A is given by the relation:

$$\begin{aligned}&\rho U_{1d}^2 h_1 W_c - \rho U_{1d}^2 \beta_{4A}^2 (h_4 W_c - A_{4Ac}) - \rho U_{1d}^2 \alpha_{4A}^2 A_{4Ac} = p_a (h_1 - h_4) W_c \\ &\quad + T_A + W_c \int_0^{h_4} [p_a + \rho g y]\, \mathrm{d}y - W_c \int_0^{h_1} [p_a + \rho g y]\, \mathrm{d}y \\ &\quad \Longrightarrow 2U_{1nd}^2 [1 - \beta_{4A} + \alpha_{2A} B_a (\beta_{4A} - \alpha_{4A})] = C_{TG} B_g - \frac{1}{Fr^2}(1 - H_4^2). \end{aligned} \tag{2.12}$$

The array-scale conservation equations, therefore, give us four additional equations, ((2.9)–(2.12)), and four additional unknown variables, which are H_4, α_{2A}, α_{4A} and β_{4A}. Together with the equation from the channel scale (2.7), there are now five equations and six unknown variables.

2.3. *Channel and array-scale friction terms*

The installation of a tidal array in a channel causes an increase in the total channel drag, which is referred to as added drag in this paper. This added drag comes from two sources. The first is directly, from the drag imparted by the turbines on the flow, its effect appears as C_{TG} in (2.7). The second is indirectly, from the cross-stream axial flow variations caused by the tidal array. The friction force in a channel depends on the flow velocity and here it is modelled to be proportional to the square of the velocity as explained in § 2.1. Consequently, the cross-stream axial flow variations, if significant, cause an increase in the friction force in the channel. This second source of added drag is non-negligible only when the array length is comparable to the channel length because only then the cross-stream axial flow variations persist for a significant proportion of the channel length to affect the total friction force. When the array length is long, such that it is comparable to the channel length, then another effect that can come into play is the friction at the array scale. In this subsection, we will include the effects of (i) the tidal array-induced axial flow variations on the friction force in the channel and (ii) the friction force on the array-scale dynamics.

Figure 3 shows a top view schematic of the channel-scale flow with the tidal array represented as a box with blockage area ratio B_a and length L_{15A}. As mentioned before, the change in the water column height along the axial direction is usually small, so we assume that the average velocity remains constant at every axial location and take it to be U_{1d} everywhere for the purpose of estimating the friction force. We make a further approximation by using average array bypass and core flow velocities throughout the array length (L_{15A}). The maximum array bypass flow velocity factor is β_{4A}, which is achieved at location 4A, and the minimum is 1, which is achieved at locations 1A and 5A. The average array bypass flow from 1A to 5A (β_b), therefore, is modelled approximately as: $\beta_b = 0.5(1 + \beta_{4A})$. In order to satisfy the conservation of mass, the average core flow from 1A to 5A (α_c) is given by the relation below.

$$\alpha_c B_a + 0.5(\beta_{4A} + 1)(1 - B_a) = 1. \tag{2.13}$$

The array length (L_{15A}) varies with the local turbine arrangement (B_l). On the one hand, for $B_l \approx 0$, i.e. when devices are very far apart from each other, there is very little interaction between the devices and the array-scale wake length will be close to the wake length for a single device. On the other hand, for $B_l \approx 1$, i.e. when devices

https://doi.org/10.1017/jfm.2017.399 Published online by Cambridge University Press

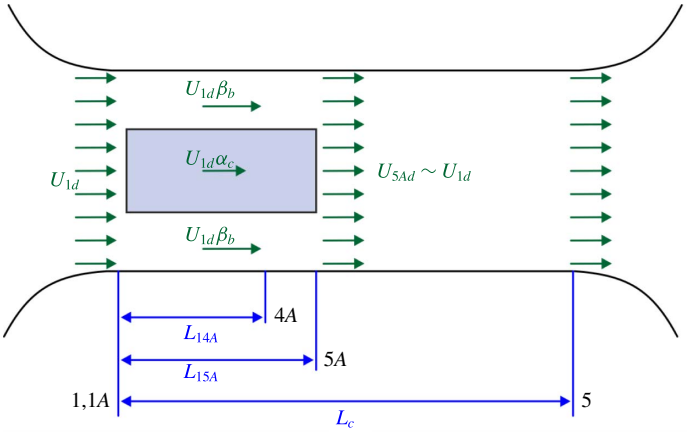


FIGURE 3. (Colour online) Top view schematic of the channel-scale flow with the tidal array represented as a box with blockage area ratio B_a.

are almost touching, the flow will see the devices as one large device and the array-scale wake length will be scaled accordingly. We assume a simple linear relation for L_{15A} at intermediate values of B_l as:

$$L_{15A} = L_{Array}\left(\frac{(n-1)B_l + 1}{n}\right), \tag{2.14}$$

where L_{Array} is the maximum length of the array that is achieved when $B_l = 1$ and L_{Array} itself depends on the global blockage. It will increase monotonically with B_g for a given channel, and we assume this increase will also be linear. In this paper, the channel length is always given in terms of the ratio $L_{A/C} = L_{Array}/L_c$ at a given B_g, and this ratio ($L_{A/C}$) changes linearly with B_g. For example, if the channel length is given as $L_{A/C} = 0.5$ at $B_g = 0.2$, then for this channel $L_{A/C} = 0.25$ at $B_g = 0.1$.

Based on the above assumptions, the friction force across the channel is given as:

$$\begin{aligned} W_c \int_0^{L_c} \tau_w \,\mathrm{d}x \;&=\; W_c \rho f_1 U_{1d}^2 (L_c - L_{15A}) + W_c B_a \rho f_1 U_{1d}^2 \alpha_c^2 L_{15A} \\ &\quad + W_c (1 - B_a) \rho f_1 U_{1d}^2 \left(\frac{1+\beta_{4A}}{2}\right)^2 L_{15A} \\ &=\; W_c \rho f_1 U_{1d}^2 \left[L_c + L_{15A}\left(B_a \alpha_c^2 + (1-B_a)\left(\frac{1+\beta_{4A}}{2}\right)^2 - 1\right)\right]. \end{aligned} \tag{2.15}$$

This friction term is then inserted in (2.5), and the resulting equation after integration and non-dimensionalisation is given as:

$$U_{1nd}^2 = \frac{C_f}{C_f + C_{fm}} - \frac{C_{TG} B_g}{C_f + C_{fm}}, \tag{2.16}$$

where $C_{fm} = (2 f_1 L_{15A}/h_1)(B_a \alpha_c^2 + (1 - B_a)((1 + \beta_{4A})/2)^2 - 1)$ is the non-dimensional tidal array-induced increase in the channel friction force. A higher value of C_{fm} means

https://doi.org/10.1017/jfm.2017.399 Published online by Cambridge University Press

a higher reduction in the incoming flow velocity U_{1nd}. It can be seen that C_{fm} is higher when the bypass flow coefficient β_{4A} and the array length L_{15A} are higher; both of these terms increase with B_l and B_g.

In order to include the friction terms in the array-scale conservation equations, we also need an estimation of the length from 1*A* to 4*A* (L_{14A}) as a fraction of L_{15A}. The length from 2*A* to 4*A*, which is the near-wake length, is known to be 2–4 times the turbine diameter (Mehta *et al.* 2014), and the length from 2*A* to 5*A*, which includes the near as well as the far-wake lengths, is known to be 6–10 times the turbine diameter (Mehta *et al.* 2014). The length from 1*A* to 2*A* is usually taken to be twice the turbine diameter (Porté-Agel *et al.* 2011). Based on these numbers, L_{14A} is 0.5–0.75 times L_{15A}. In this paper, we assume $L_{14A} = 0.7L_{15A}$. The friction force from 1*A* to 4*A* is then given as:

$$W_c \int_0^{L_{14A}} \tau_w \, \mathrm{d}x = W_c \rho f_1 U_{1d}^2 L_{14A} \left(B_a \alpha_c^2 + (1 - B_a) \left(\frac{1 + \beta_{4A}}{2} \right)^2 \right). \tag{2.17}$$

This term is substituted into (2.12) (momentum conservation between 1*A* and 4*A*), which becomes:

$$2U_{1nd}^2[1 - \beta_{4A} + \alpha_{2A} B_a (\beta_{4A} - \alpha_{4A})] = U_{1nd}^2 C_{fm2} + C_{TG} B_g - \frac{1}{Fr^2}(1 - H_4^2), \tag{2.18}$$

where $C_{fm2} = (2f_1 L_{14A}/h_1)(B_a \alpha_c^2 + (1 - B_a)((1 + \beta_{4A})/2)^2)$ is the non-dimensional friction force at the array scale. This term increases with β_{4A}, L_{14A} and f_1.

This second additional friction term (C_{fm2}) also affects the array-scale core and bypass flow energy equations. The effect of friction is to create shear in the entire flow such that energy gets dissipated everywhere. This dissipation is given as the friction force multiplied by the velocity flux. This means that the dissipation in the array-scale core and bypass flow will be given by multiplying the friction force, C_{fm2}, by $U_{1d} \alpha_{2A} B_a W_c h_1$ and $U_{1d} W_c h_1 (1 - \alpha_{2A} B_a)$, respectively. The energy equations in the array-scale core and bypass flows between 1*A* and 4*A*, which were given by (2.10) and (2.11), respectively, are now given as:

$$U_{1nd}^2 (1 - \alpha_{4A}^2) + \frac{2}{Fr^2}(1 - H_4) = B_l C_{TG} + U_{1nd}^2 C_{fm2}, \tag{2.19}$$

$$1 - H_4 = \frac{Fr^2}{2} U_{1nd}^2 [(\beta_{4A}^2 - 1) + C_{fm2}], \tag{2.20}$$

where (2.20) is equivalent to the Darcy–Weisbach equation, which is a phenomenological equation used for estimating head loss in a pipe or a channel with wall friction. This equation also shows that C_{fm2} causes a reduction in H_4, and therefore makes the flow through the turbines faster and thus increases the power generation. It seems counter-intuitive that friction is causing an increase in power generation. However, it must be noted that for a given tidal head, the increase in channel friction will also cause a reduction in the incoming flow velocity (2.16) and so the overall effect will be a reduction in power generation.

Lastly, we modify the definition of the global power coefficient (C_{PG}), given in (2.1), to:

$$C_{PG} = \frac{P_D}{\frac{1}{2}\rho U_{5A}^3 A_d} = \frac{nP_D}{\frac{1}{2}\rho U_{5A}^3 n A_d}, \tag{2.21}$$

https://doi.org/10.1017/jfm.2017.399 Published online by Cambridge University Press

where U_{5A} is the flow velocity through location $5A$ when turbines are not present in the channel. This change is to account for the increase in the flow through the turbines because of their placement in the channel.

The introduction of these two effects – the tidal array-induced increase in the channel friction and the friction at the array scale – therefore gives us an additional variable α_c and an additional equation (2.13). Further to this, the channel and array-scale momentum equations, and the array-scale core and bypass flow energy equations are replaced by (2.16), (2.18), (2.19) and (2.20), respectively.

2.4. *Device-scale conservation equations*

The device scale is between locations $1L$ and $5L$ as marked in figure 2. We assume that the length of the device-scale region is small enough for the effects of friction to be ignored. The flow through the individual devices is separated by the dashed lines and comprises of the device-scale core and bypass flows (shown in figure 2*b*). The dimensions of the device-scale flow width and vertical height at locations $1L$ and $4L$ are given in terms of the array-scale area factors (m_1, k_1, m_4 and k_4) (shown in figure 2*b*,*c*). These factors are modelled empirically in § 2.5. At the upstream location, $1L$, the velocity ($U_{1L} = m_1 k_1 U_{1d} \alpha_{2A}$) and channel height ($h_{1L}$) are both uniform across the local passage. Locations U and D are the positions immediately upstream and downstream of the turbines, respectively. The average values of the device-scale variables at the turbine location have subscript $2L$. The location downstream of the turbines where the channel height (h_{4L}) is uniform across the local passage width (L_d/k_4) but the flow velocity is still varying is marked $4L$. Location $5L$ is further downstream in the channel after the device-scale wake mixing is completed. The channel height and flow velocity are both uniform across the local passage width at this location.

Mass conservation between $1L$ and $4L$ gives:

$$\beta_{4L} = \frac{1 - \alpha_{2L} B_l}{1 - \dfrac{\alpha_{2L}}{\alpha_{4L}} B_l}, \tag{2.22}$$

where α_{2L} is the local core flow velocity coefficient at the array location and α_{4L} and β_{4L} are the local core and bypass flow velocity coefficients at $4L$, respectively.

Energy conservation in the local core flow between $1L$ and $4L$ gives:

$$\begin{aligned} &\frac{1}{2}\rho(m_4 k_4 U_{1d} \alpha_{2A} \alpha_{4L})^3 A_{4Lc} - \frac{1}{2}\rho(m_1 k_1 U_{1d} \alpha_{2A})^3 A_{1Lc} + P_D \\ &\quad = m_1 k_1 U_{1d} \alpha_{2A} A_{1Lc} p_{avg1L} - m_4 k_4 U_{1d} \alpha_{2A} \alpha_{4L} A_{4Lc} p_{avg4L} \\ &\qquad \Longrightarrow U_{1nd}^2 \alpha_{2A}^2 [(m_1 k_1)^2 - (m_4 k_4)^2 \alpha_{4L}^2] + \frac{2}{Fr^2}(H_{1L} - H_{4L}) = C_{TG}, \end{aligned} \tag{2.23}$$

where P_D is the useful power extracted from the flow by a single turbine and $H_{1L} = h_{1L}/h_1$ and $H_{4L} = h_{4L}/h_1$ are the non-dimensional heights across the device scale at $1L$ and $4L$, respectively. A_{1Lc} and A_{4Lc} are local core flow areas at $1L$ and $4L$, respectively, and are given as:

$$A_{1Lc} = \frac{A_d}{m_1 k_1} \alpha_{2L}, \quad A_{4Lc} = \frac{A_d}{m_4 k_4} \frac{\alpha_{2L}}{\alpha_{4L}}. \tag{2.24a,b}$$

https://doi.org/10.1017/jfm.2017.399 Published online by Cambridge University Press

The terms p_{avg1L} and p_{avg4L} are the average pressures in the local flow passage at $1L$ and $4L$, respectively, and are approximated by the hydrostatic pressure at the midpoint of the core flow at $1L$ and $4L$ as:

$$p_{avg1L} = [p_a + \rho g(h_{1L} - h_T)], \quad p_{avg4L} = [p_a + \rho g(h_{4L} - h_T)]. \tag{2.25a,b}$$

Energy conservation in the local bypass flow between $1L$ and $4L$ gives:

$$\begin{aligned} &\frac{1}{2}\rho(m_4k_4U_{1d}\alpha_{2A}\beta_{4L})^3\left(\frac{A_l}{m_4k_4} - A_{4Lc}\right) - \frac{1}{2}\rho(m_1k_1U_{1d}\alpha_{2A})^3\left(\frac{A_l}{m_1k_1} - A_{1Lc}\right) \\ &\quad = U_{1d}\alpha_{2A}\left[m_1k_1\left(\frac{A_l}{m_1k_1} - A_{1Lc}\right)p_{avg1L} - m_4k_4\alpha_{4L}\left(\frac{A_l}{m_4k_4} - A_{4Lc}\right)p_{avg4L}\right] \\ &\quad \Longrightarrow \frac{2}{Fr^2}(H_{1L} - H_{4L}) = U_{1nd}^2\alpha_{2A}^2[(m_4k_4\beta_{4L})^2 - (m_1k_1)^2]. \end{aligned} \tag{2.26}$$

The term $H_{1L} - H_{4L}$ is eliminated by combining the device-scale core flow and bypass flow energy equations ((2.23) and (2.26)). The resulting equation is:

$$U_{1nd}^2\alpha_{2A}^2(m_4k_4)^2[\beta_{4L}^2 - \alpha_{4L}^2] = C_{TG}. \tag{2.27}$$

Momentum conservation for the local passage between $1L$ and $4L$ gives:

$$\begin{aligned} T_D \;=\; & p_{avg1L}\frac{A_l}{m_1k_1} - p_{avg4L}\frac{A_l}{m_4k_4} + p^*A_{14L}^* + \rho(m_1k_1U_{1d}\alpha_{2A})^2\frac{A_l}{m_1k_1} \\ & - \rho(m_4k_4U_{1d}\alpha_{2A}\alpha_{4L})^2A_{4Lc} - \rho(m_4k_4U_{1d}\alpha_{2A}\beta_{4L})^2\left(\frac{A_l}{m_4k_4} - A_{4Lc}\right) \\ & \Longrightarrow \frac{(m_4k_4)^2}{2}(\beta_{4L}^2 - \alpha_{4L}^2) = \frac{m_1k_1}{Bl} - m_4k_4\alpha_{4L}\alpha_{2L} - \frac{m_4k_4\beta_{4L}^2}{Bl} \\ & + m_4k_4\beta_{4L}^2\frac{\alpha_{2L}}{\alpha_{4L}} + \frac{1}{2Blm_4k_4}[(m_4k_4\beta_{4L})^2 - (m_1k_1)^2]. \end{aligned} \tag{2.28}$$

The term $p^*A_{14L}^*$ is the pressure force term arising from the non-zero axial projection of the lateral surface area between $1L$ and $4L$. This term is modelled in the same way as in Nishino & Willden (2013):

$$p_{avg1L}\frac{A_l}{m_1k_1} + p^*A_{14L}^* = p_{avg1L}\frac{A_l}{m_4k_4}. \tag{2.29}$$

The resulting equation then is written as:

$$\begin{aligned} \frac{(m_4k_4)^2}{2}(\beta_{4L}^2 - \alpha_{4L}^2) \;=\; & \frac{m_1k_1}{B_l} - m_4k_4\alpha_{4L}\alpha_{2L} - \frac{m_4k_4\beta_{4L}^2}{B_l} + m_4k_4\beta_{4L}^2\frac{\alpha_{2L}}{\alpha_{4L}} \\ & + \frac{1}{2B_lm_4k_4}[(m_4k_4\beta_{4L})^2 - (m_1k_1)^2]. \end{aligned} \tag{2.30}$$

The device-scale conservation equations therefore give us 3 additional model equations, these are (2.22), (2.27) and (2.30). The new variables introduced are α_{2L}, α_{4L} and β_{4L}, as well as the products m_1k_1 and m_4k_4 which are the array-scale area factors.

Having considered the conservation equations over the channel, array and device scales, we have nine equations and twelve unknown variables. In order to close the equations, we now derive three additional equations based on empirical models. These equations govern the drag of the turbines and the array-scale area factors.

https://doi.org/10.1017/jfm.2017.399 Published online by Cambridge University Press

2.5. *Empirically modelled equations necessary for closure*

The turbines are modelled empirically in terms of a local induction factor (a), which is defined as the ratio of the deceleration in the local core flow velocity between $1L$ and $2L$ to the local core flow velocity at $1L$:

$$a = \frac{m_1 k_1 \alpha_{2A} U_{1d} - \alpha_{2A}\alpha_{2L} U_{1d}}{m_1 k_1 \alpha_{2A} U_{1d}} = 1 - \frac{\alpha_{2L}}{m_1 k_1}. \tag{2.31}$$

A higher value of induction factor implies that more drag is imparted on the flow by the turbines. This parameter will be used as the turbine tuning parameter in this paper.

The other empirically modelled quantities are the array-scale area factors m_1, k_1, m_4 and k_4. These factors quantify the expansion in the array core flow between $1L$ and $4L$. Because these factors only appear as products, $m_1 k_1$ and $m_4 k_4$, in the equations, they are modelled together as:

$$\left.\begin{aligned} m_1 k_1 &= \left[1 + \left(\frac{1}{n}\right)(\alpha_{2A} - 1)\right]^{-1}, \\ m_4 k_4 &= \left[1 + \left(\frac{1}{n}\right)\left(\frac{\alpha_{2A}}{\alpha_{4A}} - 1\right)\right]^{-1}. \end{aligned}\right\} \tag{2.32}$$

This model for the array-scale expansion factors is given by Nishino & Willden (2013). For $n \to \infty$, the array scale is much bigger than the device scale, and therefore, $m_1 k_1$ and $m_4 k_4$ both approach 1. For $n = 1$, the array scale and device scale are the same, and therefore, $m_1 k_1 = 1/\alpha_{2A}$ and $m_4 k_4 = \alpha_{4A}/\alpha_{2A}$. For intermediate values of n, equation (2.32) gives empirical power laws for these area factors.

The final list of 12 equations in terms of 12 unknown variables is given in appendix A. The channel parameters – the inherent drag coefficient (C_f), the channel length (L_c) and the Froude number (Fr) – are constant for a given tidal channel. The design parameters – the global blockage (B_g), the local blockage (B_l) and the induction factor (a) – can be varied in order to maximise the power extracted per turbine (C_{PG}). This final set of equations is solved using a Newton–Raphson method. Python is used for the numerical calculations.

3. Results

As mentioned before, the present model combines three effects: the effect of local blockage, the effect of surface deformation and the effect of added drag. In this section, we present these three effects separately for arrays of $n = 16$ turbines. The choice of the number of turbines is fixed and arbitrary. The effect of n is modelled empirically in exactly the same manner as in Nishino & Willden (2013) using (2.32). In § 4, the importance of considering the three effects in combination will be discussed.

3.1. *The effect of local blockage*

The results in this section are equivalent to those in Nishino & Willden (2012*b*, 2013), and show the same trends as they observed. These results are included here as a baseline against which the effects of surface deformation and added drag can be assessed. The channel parameters are set to $Fr = 0$, $1/C_f = 0$ and $L_{A/C} = 0$, so that surface deformation and added drag effects are absent. The focus here is on

https://doi.org/10.1017/jfm.2017.399 Published online by Cambridge University Press

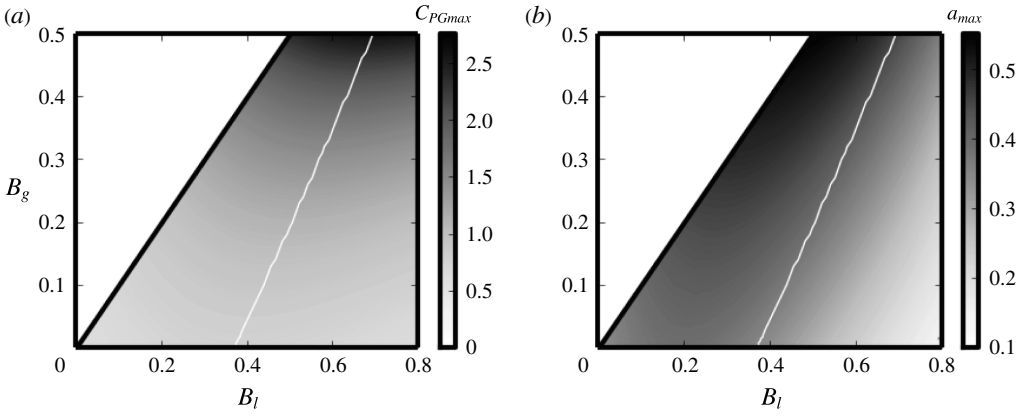


FIGURE 4. (*a*) C_{PGmax} and (*b*) a_{max} as functions of B_l and B_g for $Fr = 0$, $1/C_f = 0$ and $L_{A/C} = 0$. C_{PGmax} is the maximum global power coefficient for given values of B_l and B_g. a_{max} is the tuned value of a required to achieve C_{PGmax}.

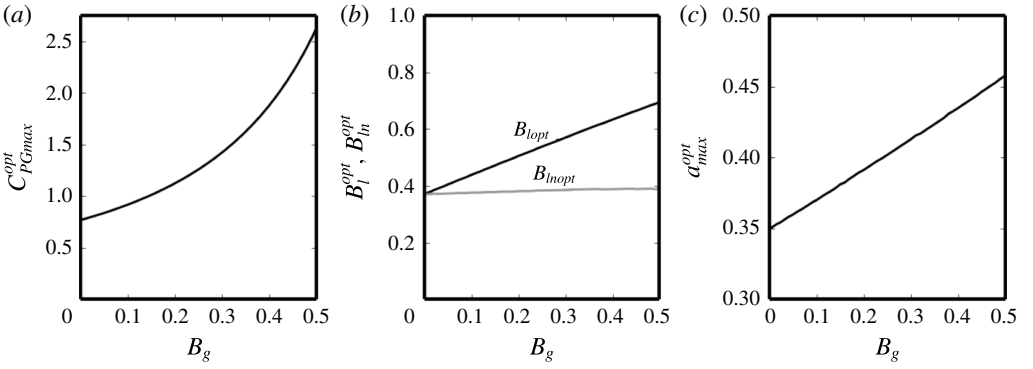


FIGURE 5. (*a*) C_{PGmax}^{opt}, (*b*) B_l^{opt} and B_{ln}^{opt} and (*c*) a_{max}^{opt} against B_g for $Fr = 0$, $1/C_f = 0$ and $L_{A/C} = 0$. It can be seen that the power extraction per turbine and the turbine resistance required to achieve it both increase with the global blockage, while the normalised optimal local blockage remains nearly unchanged.

maximising the power extraction per turbine (C_{PG}) by adjusting the arrangement of the turbines (through B_l) and the turbine resistance (through a). Figure 4 presents (*a*) C_{PGmax} and (*b*) a_{max} as functions of B_l and B_g for the modelled array. Here, C_{PGmax} refers to the maximum C_{PG} for a given B_l and B_g. The tuned value of a required to achieve C_{PGmax} is referred to as a_{max}. The thin white lines in the plots correspond to the optimal local blockage (B_l^{opt}), which is the value of local blockage required for maximum power extraction at a given global blockage (C_{PGmax}^{opt}). The value of a_{max} at B_l^{opt} is referred as a_{max}^{opt}.

Figure 5 shows the variation of (*a*) C_{PGmax}^{opt}, (*b*) B_l^{opt} and B_{ln}^{opt} and (*c*) a_{max}^{opt} against B_g. Here, $B_{ln} = (B_l - B_g)/(1 - B_g)$ is a normalised local blockage such that it varies from 0 to 1 when B_l varies from B_g to 1 and $B_{ln}^{opt} = (B_l^{opt} - B_g)/(1 - B_g)$. Figure 5(*a*) shows that C_{PGmax}^{opt} increases with B_g; this is because of the blockage effect which causes C_{PG} to cross the Lanchester–Betz limit. A consequence of this phenomenon is that higher global blockage is desirable for increasing the power extraction per turbine.

https://doi.org/10.1017/jfm.2017.399 Published online by Cambridge University Press

In addition, figure 5(*b*,*c*) shows that both B_l^{opt} and a_{max}^{opt} increase with increasing B_g. This implies that more densely packed turbines with higher resistance are desirable in higher blockage cases.

The most important observation from these results is that the internal arrangement of turbines can be adjusted to an optimal value (B_l^{opt}) to increase the power extraction per turbine. Nishino & Willden (2012*b*) explained this in terms of two competing effects. The first is that as the turbines are moved closer together, the increase in local blockage increases β_{4L} and hence increases C_{PG}. This is similar to the way in which the global blockage effect increases β_{4A} and hence increases C_{PG}. The second is that as the turbines are moved closer together, they start to block the flow through the array, i.e. the turbines cause a reduction in α_{2A}, which decreases C_{PG}. In between these two competing effects there is an optimum value of local blockage (B_l^{opt}) which will give the maximum power extraction per turbine at a given global blockage (C_{PGmax}^{opt}).

In this paper, we observe that this optimal local blockage, when normalised as B_{ln}^{opt}, is a very weak function of B_g as it remains almost constant at $B_{ln}^{opt} = 0.37$–0.39 when B_g is varied from 0.005 to 0.5. This means that regardless of the global blockage, the optimum local arrangement of turbines within the array remains the same. In other words, the optimal free area in a tidal array ($1 - B_l^{opt}$) is always approximately 60 % of the maximum free area allowed in the channel ($1 - B_g$). It is to be noted, however, that the existence of a nearly constant value of B_{ln}^{opt} is true only in the present model in which there is no near-wake mixing (between $2L$ and $4L$) regardless of the amount of shear created by the devices (i.e. the difference between β_{4L} and α_{4L}). This assumption will begin to break down in marine flows with high turbulence intensity.

3.2. *The effect of surface deformation*

When the flow passes through an array of turbines, they extract power from the flow. Consequently, the potential energy of the flow decreases downstream of the turbines. This reduction in the potential energy causes the water column height to drop, and this drop (or surface deformation) is proportional to the square of the Froude number as shown in (2.11). The effect of surface deformation is explored here by varying the Froude number of the incoming flow. The inherent channel drag coefficient is set to $1/C_f = 0$ and the ratio of array length to channel length is set to $L_{A/C} = 0$ to exclude the effect of added drag. Figure 6 shows the variation of (*a*) C_{PGmax}^{opt}, (*b*) B_l^{opt} and (*c*) a_{max}^{opt} with Fr, which is the Froude number of the undisturbed flow, for several values of B_g. Figure 6(*a*) shows that the surface deformation increases the power extraction per turbine. In addition, figures 6(*b*) and 6(*c*), respectively, show that the surface deformation also increases the local blockage and turbine resistance required to achieve the maximum power extraction per turbine.

The reason for this increase in C_{PGmax}^{opt}, B_l^{opt} and a_{max}^{opt} with the surface deformation is that the drop in the water column height amplifies the blockage effect. The effect of surface deformation is higher with higher B_g and the slope of variation is steeper with higher Fr. For the case with the highest variation ($B_g = 0.3$), the changes in B_l^{opt} and a_{max}^{opt} associated with an increase in Fr from 0 to 0.3 are approximately 10 % and 5 %, respectively.

In summary, like Whelan *et al.*'s (2009) model, this paper shows (i) that power extraction increases with Froude number and (ii) that higher turbine resistance is desirable in higher Froude number cases. We additionally show that a higher local blockage is desirable in the higher Froude number cases. All these changes, however, are small over the range of Froude numbers found in typical marine flows ($Fr \approx 0.1$–0.2).

https://doi.org/10.1017/jfm.2017.399 Published online by Cambridge University Press

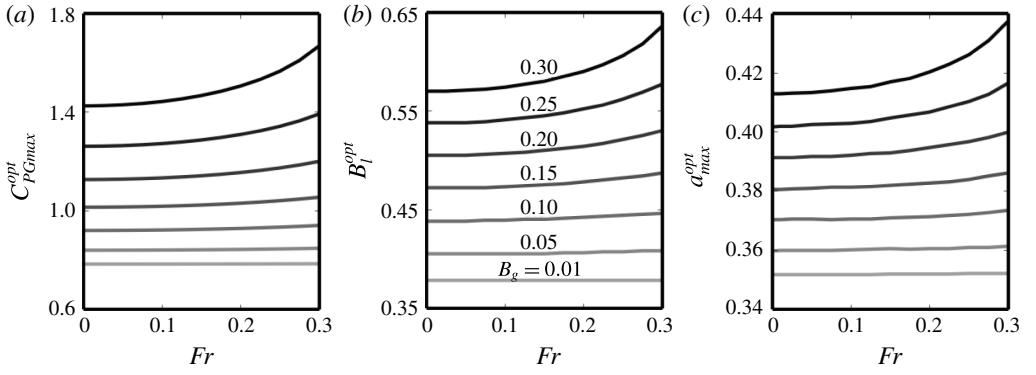


FIGURE 6. Variation of (*a*) C_{PGmax}^{opt}, (*b*) B_l^{opt} and (*c*) a_{max}^{opt} with Fr and B_g ($1/C_f = 0$ and $L_{A/C} = 0$). The surface deformation, which is proportional to Fr^2, increases the blockage effect slightly. Consequently, all three quantities increase slightly with Fr.

3.3. *The effect of added drag from the installation of the tidal array*

Figure 5(*a*) shows that the power extraction per turbine always increases when the fraction of the channel covered by turbines (B_g) increases, and that the variation is faster than a linear variation. This, however, is not the case in realistic channels because of the effect of added drag from the array itself. The added drag decreases the incoming flow velocity (U_{1d}), as shown in (2.7) and (2.16), and therefore has the effect of reducing the power extraction. As explained in § 2.3, the added drag comes from two sources – directly, from the drag imparted by turbines on the flow (C_{TG}) and indirectly, from the tidal array-induced axial flow variations that increase the channel friction (C_{fm}). The first term (C_{TG}) is the main contributor to the added drag, and the second term (C_{fm}) is relatively small and comes into play only when $L_{A/C}$ is large. When $L_{A/C}$ is large, a third effect comes into play: the friction force at the array scale (C_{fm2}).

In order to investigate these effects, we fix the Froude number at $Fr = 0.1$ and vary the value of $1/C_f$ from 0.15 to 0.95. The lower limit of $1/C_f$ as 0.15 is set to keep ΔH smaller than 0.05 (the model assumes that ΔH is small – § 2.1) and the upper limit is set as 0.95 to keep the seabed friction term ($f_1 L_c/h_1$) small. At first, we also set the channel length to be much higher than the array length ($L_{A/C} = 0$). This means that the effects of C_{fm} and C_{fm2} are both negligible. Figure 7 shows the variation of (*a*) C_{PGmax}^{opt}, (*b*) B_l^{opt} and (*c*) a_{max}^{opt} with $1/C_f$ for several values of B_g. The variation is more significant with higher B_g and the slope of variation is steeper with smaller values of $1/C_f$.

In the absence of the added drag effect (when $1/C_f$ is small), the blockage effect always increases the power extraction per turbine. Figure 7(*a*) shows that this blockage effect diminishes as $1/C_f$ increases. With higher values of $1/C_f$, the advantage of increasing B_g is partially nullified by the increase in the relative contribution of the turbines towards the total channel drag. Beyond a certain value of $1/C_f$ – approximately 0.8 for the channel modelled here – the power extraction per turbine actually starts to decrease with increasing B_g.

Figure 7(*b*) shows that B_l^{opt} is almost independent of $1/C_f$, although there is a very small increase with increasing $1/C_f$. Later we will see that this is true only when $L_{A/C} \approx 0$. When the array length is comparable to the channel length then the size of

https://doi.org/10.1017/jfm.2017.399 Published online by Cambridge University Press

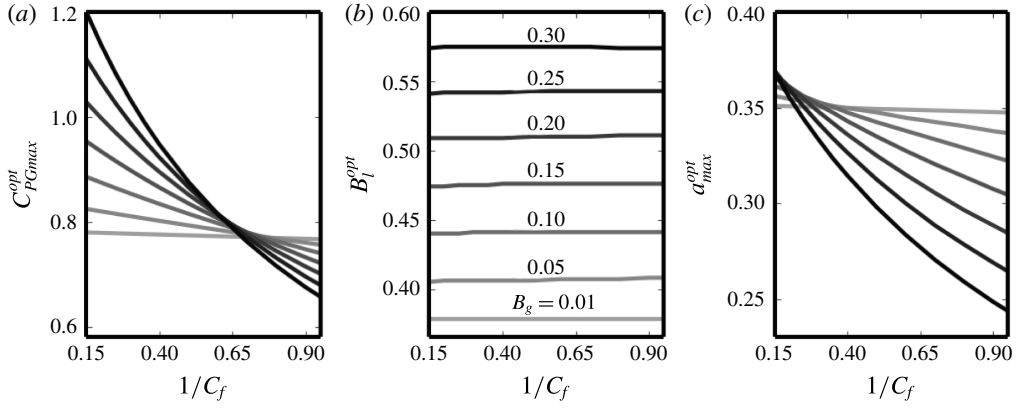


FIGURE 7. Variation of (*a*) C_{PGmax}^{opt}, (*b*) B_l^{opt} and (*c*) a_{max}^{opt} with $1/C_f$ and B_g for $Fr = 0.1$ and $L_{A/C} = 0$. The effect of added drag from the turbines is small at $1/C_f = 0.15$ and increases monotonically with $1/C_f$. It can be seen that both the power extraction and the turbine resistance required to achieve it reduce because of the effect of added drag. The optimal local blockage, however, is not affected by the effect of added drag when $L_{A/C} = 0$.

the array (and hence B_l) becomes important as explained in § 2.3, i.e. the effect of C_{fm} and C_{fm2} will change B_l^{opt}. This finding could be inferred from the results in Garrett & Cummins (2013) where they show the effect of the size of a tidal array on power extraction.

Figure 7(*c*) shows that the optimal turbine resistance (a_{max}^{opt}) decreases with increasing $1/C_f$. This is because as $1/C_f$ increases, the contribution of turbines to the total channel drag is no longer negligible, and this additional drag therefore starts to reduce the power extracted by the array. It can also be seen that, at small values of $1/C_f$, higher turbine resistance is desirable when the global blockage is higher. Beyond a certain value of $1/C_f$ – 0.3 for the channel modelled here – however, a_{max}^{opt} actually decreases with increasing global blockage.

When the channel length is comparable to the array length, i.e. $L_{A/C}$ can no longer be taken to be approximately 0, the effects of C_{fm} (added channel friction due to the array) and C_{fm2} (friction at the array scale) come into play. The effects of both C_{fm} and C_{fm2} increase with friction (C_f) and the length of the array (L_{15A}), and for a given $L_{A/C}$ the length of the array increases with the local blockage (B_l) as explained in § 2.3. On the one hand, C_{fm} adds to the channel drag, which reduces the incoming flow velocity and hence adversely affects the power generation. Its effect, therefore, brings the optimal local blockage (B_l^{opt}) to a lower value than that of the $L_{A/C} = 0$ case. On the other hand, C_{fm2} causes higher surface deformation at the array scale, which increases the flow through the turbines, and hence favourably affects the power generation. Its effect, therefore, brings the optimal local blockage (B_l^{opt}) to a higher value than that of the $L_{A/C} = 0$ case. The result of these two competing effects on B_l^{opt} then depends upon whether the C_{fm} or C_{fm2} term dominates.

In order to investigate the effect of C_{fm} and C_{fm2}, figure 8 presents the variation of (*a*,*d*) C_{PGmax}^{opt}, (*b*,*e*) B_l^{opt} and (*c*,*f*) a_{max}^{opt} with $1/C_f$ for various values of $L_{A/C}$ with $B_g = 0.1$ (*a*–*c*) and $B_g = 0.3$ (*d*–*f*). It can be seen from the trends in B_l^{opt} in figures 8(*b*) and 8(*e*) that the effects of C_{fm} and C_{fm2} increase with decreasing $1/C_f$ and increasing $L_{A/C}$. It can also be seen from figures 8(*b*) and 8(*e*) that B_l^{opt} first decreases with

https://doi.org/10.1017/jfm.2017.399 Published online by Cambridge University Press

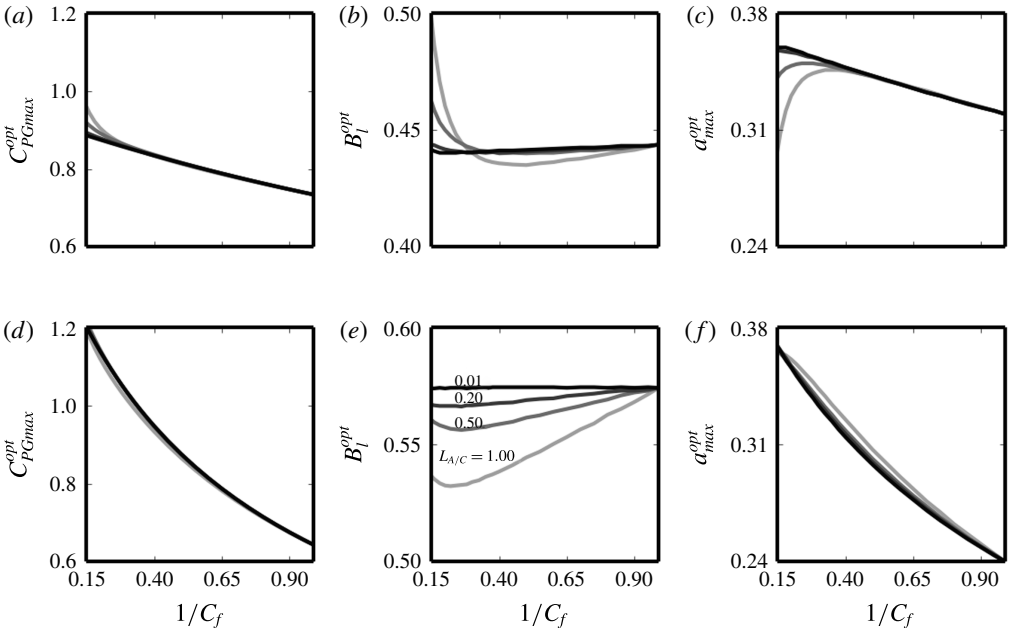


FIGURE 8. Variation of (*a*,*d*) C^{opt}_{PGmax}, (*b*,*e*) B^{opt}_{l} and (*c*,*f*) a^{opt}_{max} with $1/C_f$ and $L_{A/C}$ for $Fr = 0.1$ and $B_g = 0.1$ (*a*–*c*) and $B_g = 0.3$ (*d*–*f*). Except at very small values of $1/C_f$ in the $B_g = 0.1$ case, B^{opt}_{l} decreases with $L_{A/C}$. The effect of $L_{A/C}$ on C^{opt}_{PGmax} and a^{opt}_{max} is relatively small.

decreasing $1/C_f$ (i.e. the effect of C_{fm} is dominant in between $1/C_f = 0.95$ and 0.3), and then increases if $1/C_f$ further reduces (i.e. the effect of C_{fm2} is dominant in between $1/C_f \approx 0.3$ and 0.15).

In the region where the effect of C_{fm} is dominant (i.e. $1/C_f$ from 0.95 to approximately 0.3), it can be noted from figures 8(*a*,*d*) and 8(*c*,*f*) that the effect of C_{fm} on C^{opt}_{PGmax} and a^{opt}_{max}, respectively, is relatively small. This is because the variation in both C^{opt}_{PGmax} and a^{opt}_{max} with $1/C_f$ is large because of the added drag effect from the turbines (C_{TG}), as shown in figure 7. The slight changes caused by the effect of C_{fm} are therefore negligible in this region. The effect of C_{fm}, therefore, is important only in determining the optimal local blockage (B^{opt}_{l}). Its effect is significant when B_g is high, the channel length is short enough to be comparable to the array length ($L_{A/C}$ is close to 1), and the seabed friction coefficient is large ($1/C_f$ is small).

In the region where the effect of C_{fm2} is dominant (i.e. $1/C_f$ from approximately 0.3 to 0.15), it can be noted from figures 8(*b*) and 8(*e*) that the effect of C_{fm2} is much more pronounced in the $B_g = 0.1$ case than in the $B_g = 0.3$ case. This is because in the higher B_g cases, C_{fm} is relatively larger and partially nullifies the effect of C_{fm2}; while in the lower B_g cases, C_{fm} is small. The steep increase in B^{opt}_{l} between $1/C_f = 0.15$ and 0.3 in the $B_g = 0.1$ case also causes C^{opt}_{PGmax} to increase (figure 8*a*) and a^{opt}_{max} to decrease (figure 8*c*) noticeably. The effect of C_{fm2} is important when B_g is small, the channel length is short enough to be comparable to the array length (i.e. $L_{A/C}$ is close to 1 even at small B_g), and the seabed friction coefficient is very large (i.e. large C_f even when L_c is small). This effect, therefore, is more likely to be important when turbines

https://doi.org/10.1017/jfm.2017.399 Published online by Cambridge University Press

are arranged in multiple rows, where the array length could well be comparable to the channel length even when B_g is small.

In summary, the effect of added drag is crucial in determining the turbine resistance required to maximise C_{PG}. A model which neglects the turbine drag will over-predict the induction factor required to maximise the power extracted (see figure 7*c*). Moreover, the added drag has to be considered in order to estimate the optimum global blockage correctly, i.e. the fraction of the channel area that should be occupied by turbines for maximum power extraction per turbine (see figure 7*a*). The installation of a tidal array causes a further increase in the channel friction by creating cross-stream variations in the axial velocity, and this effect leads to a lower optimal local blockage than would otherwise be expected (see figure 8*b*,*e*). This is true except when the effect of friction at the array scale becomes important, i.e. very large C_f, $L_{A/C} \approx 1$ and small B_g. In such cases, a much higher optimal local blockage is desirable than in the case where $L_{A/C}$ is negligible (see figure 8*b*). The effect of seabed friction at the array scale also reduces the optimal turbine induction factor (see figure 8*c*).

4. Discussion

As explained in § 1, it is the consideration of the effects of local blockage, surface deformation and added drag from the tidal array simultaneously in one model that sets our model apart from those in the literature. The individual effects are discussed in § 3, and are comparable to those given by the previously verified models of Whelan *et al.* (2009), Vennell (2010) and Nishino & Willden (2013). In this section, we focus on the importance of considering the various effects simultaneously before discussing the limitations of the present model and suggesting potential improvements.

4.1. *Combined effect*

Nishino & Willden's (2013) model shows that the local blockage in a tidal array can be adjusted to optimise the power extraction per turbine. Their model can, therefore, be used to obtain the optimum local blockage (B_l^{opt}) and the corresponding optimum turbine resistance (a_{max}^{opt}) in a tidal array. A major limitation in their model, however, is that they ignore the channel parameters, including the Froude number and the channel drag coefficient. Such a model, therefore, cannot account for the effects of surface deformation or of the added drag from the tidal array.

The model presented in this paper has shown that the surface deformation effect is small, but that the added drag effect can be significant. We have shown that neglecting the added drag can give significantly higher values of turbine tuning and slightly higher local blockage than that required to achieve the optimum performance (see figures 7*c* and 8*b*,*e*). We have also shown that when the channel length is short enough to be comparable to the array length, then the effect of friction at the array scale also comes into play. In some extreme cases, when C_f is very large, $L_{A/C}$ is close to 1, and B_g is small (i.e. very high channel friction coefficient f_1), this effect leads to a sharp increase in the optimal local blockage (see figure 8*b*) and a decrease in the optimal turbine resistance (see figure 8*c*). As mentioned before, this effect is more likely to be important when multiple rows are considered and hence the array length is large even when B_g is small.

More importantly, because Nishino & Willden's (2013) model does not account for the added drag effect, it gives a monotonic increase in power extraction per turbine with global blockage. Consequently, it cannot be used to predict up to what limit a

https://doi.org/10.1017/jfm.2017.399 Published online by Cambridge University Press

channel should be occupied by turbines for maximum power extraction per turbine. In the present model, we include the effect of added drag caused by the installation of a tidal array in a channel. This effect of added drag is more pronounced in channels with lower inherent drag, i.e. in channels with higher $1/C_f$ values. It was shown in figure 7(*a*) that C_{PGmax}^{opt} decreases with increasing $1/C_f$. This decrease is more marked in cases with higher global blockage. Consequently, beyond $1/C_f = 0.8$ in the present model, C_{PGmax}^{opt} starts to decrease with B_g.

In order to investigate the combined effect of the local blockage and added drag, figure 9(*a–c*) shows the variation of C_{PGmax} with B_{ln} and B_g for $1/C_f = 0.15$, 0.50 and 0.80, respectively, at $Fr = 0.1$ and for a channel such that $L_{A/C} = 1$ when $B_g = 0.3$ (i.e. $L_{A/C} = 1/6$ when $B_g = 0.05$, $L_{A/C} = 1/3$ when $B_g = 0.1$, and so on for the other B_g values using the linear relationship explained in § 2.3). These plots show that the optimum global blockage, i.e. the value of B_g at which the power extraction per turbine is maximised, is determined by the combined effect of the added drag and the local blockage. The optimum global blockages required in the three cases are (*a*) $B_g \approx 1.00$, (*b*) $B_g \approx 0.55$ (results not shown here for such high B_g values) and (*c*) $B_g < 0.05$. If the effect of added drag alone is considered without exploring the effect of local blockage, as in the model given by Vennell (2010), then the resultant optimum B_g would be much higher. Those results will correspond to $B_{ln} = 0$ in these plots, for which the optimum B_g in the three cases are (*a*) $B_g = 1.00$, (*b*) $B_g = 1.00$ and (*c*) $B_g \approx 0.25$.

The dots in the plots show the optimal local blockage required for C_{PGmax}^{opt}. It can be seen that B_{ln}^{opt} decreases with B_g instead of slightly increasing as was shown in figure 5, when the effect of local blockage was considered in isolation. This reduction in B_{ln}^{opt} with B_g is because of the effect of the tidal array-induced increase in channel friction (C_{fm}).

Figure 9(*d–f*) shows the variation of a_{max} with B_{ln} for different values of $1/C_f$ (with the same values of B_g, $1/C_f$ and $L_{A/C}$ as in figure 9(*a–c*)). These plots show that for any global blockage value, the turbine tuning (a_{max}) required to achieve C_{PGmax} is always lower at the optimum local blockage ($B_{ln} \approx 0.38$) than at $B_{ln} = 0$. To understand the significance of this result, consider that the power wasted by the array is the difference between the power extracted by the array ($P_A = T_A U_{1d} \alpha_{2A}$) and the power extracted by the turbines ($nP_D = nT_d U_{1d} \alpha_{2A} \alpha_{2L} = T_A U_{1d} \alpha_{2A} \alpha_{2L}$). The relative power wastage, therefore is $(P_A - nP_D)/P_A = 1 - \alpha_{2L}$, which is approximately equal to the value of a $(1 - \alpha_{2L}/m_1 k_1)$. This means that exploring the local blockage effect not only increases the power extraction per turbine but also reduces the proportion of the power wasted by the array arrangement.

In summary, figure 9 shows that considering the added drag alone and not exploring the effect of local blockage leads to over-predictions of both the global blockage (B_g) and the turbine resistance (a) for maximum power extraction per turbine. Figure 9(*a–c*) shows that the value of B_g for optimum C_{PGmax} is higher at $B_{ln} = 0$ than at B_{lnopt} (i.e. at $B_{ln} \approx 0.38$). Similarly, figure 9(*d–f*) shows that the value of a_{max} required to achieve C_{PGmax} is also higher at $B_{ln} = 0$ than at B_{lnopt}. We have already seen from figure 7 that not considering the effect of added drag, i.e. assuming large C_f or small $1/C_f$, also leads to a higher value of a than that required for maximum power extraction per turbine and shows, incorrectly, a monotonic increase in C_{PG} with B_g. This means that ignoring either of the two effects – added drag or local blockage – leads to higher B_g and a than the optimum, which in turn leads to unnecessary addition of extra turbines and higher power wastage.

https://doi.org/10.1017/jfm.2017.399 Published online by Cambridge University Press

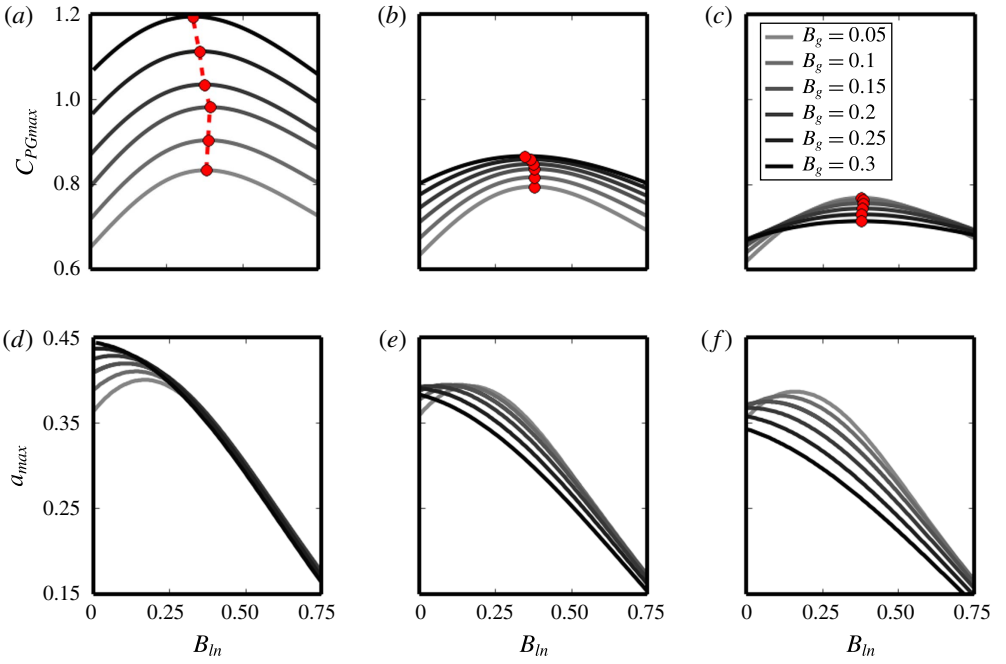


FIGURE 9. (Colour online) Variation of (*a–c*) C_{PGmax} and (*d–f*) a_{max} against B_{ln} and B_g at $Fr = 0.1$ and (*a*,*d*) $1/C_f = 0.15$, (*b*,*e*) $1/C_f = 0.5$ and (*c*,*f*) $1/C_f = 0.8$ for the channel length such that $L_{A/C} = 1$ when $B_g = 0.3$. Vennell's (2010) model is approximately equivalent to $B_{ln} = 0$, i.e. $B_l = B_g$.

Surface deformation effects are not considered in this section and the Froude number is kept fixed at 0.1. This is because the surface deformation effects are small over the range of Froude numbers applicable to most tidal energy sites ($Fr = 0.1 - 0.2$). Moreover, the surface deformation effect simply means that slightly higher B_g, B_l, and a values are required for optimal performance in higher Froude number cases. This means that Froude number can be considered independently of the other parameters without any adverse effect on the optimised array design.

4.2. *Model limitations and future improvements*

Although our model considers the above mentioned three effects simultaneously, there are a number of other effects that are not considered here. The main limitation of our model is that we have ignored the effect of several flow parameters, such as Reynolds number, turbulence intensity and velocity and density profiles. Further to this, our turbine tuning parameter does not capture the complexity of a real turbine's operations. There is, for example, no consideration of the swirl imparted on the flow by each turbine. These flow parameters and the amount of swirl in the flow will have a major impact on the wake mixing process.

Wake mixing plays an important role in the functioning of turbines – Reynolds-averaged Navier–Stokes (RANS) simulations undertaken by Nishino & Willden (2012*a*) showed that mixing increased the power extraction. To understand its role, consider that as the turbines come closer together, our model predicts that the speed of the local bypass flow between the turbines increases relative to that of the local

https://doi.org/10.1017/jfm.2017.399 Published online by Cambridge University Press

core flow. This local blockage effect then increases the power extraction by the turbines. The creation of this velocity difference in the flow at the turbine location is dependent upon the wake mixing in the downstream region. In the present model (as in Nishino & Willden's (2013) model) it is assumed that (i) there is no near-wake mixing (between locations $2L$ and $4L$) and (ii) the far-wake mixing is completed before location $4A$ regardless of the amount of velocity difference created at the turbine location.

These assumptions are not completely satisfied in a real flow. Additionally, as mentioned in § 2.2, the array-scale and device-scale vertical mixing processes are likely to happen in the same region rather than separately as assumed in the present model. Nishino & Willden (2013) also found that many of the discrepancies between their model and RANS simulations are caused by discrepancies in the wake mixing. Further work is therefore required to understand how different flow features affect the wake mixing process and hence the power extraction by the turbines.

Turbines are modelled as porous discs in the present model. They, however, are far more complex in reality. The most important difference is that a real turbine consists of blades which rotate such that the flow at the upstream face has a higher pressure than the flow at the downstream face of the blades. This pressure difference, which creates the power, depends up on the lift and drag coefficients of the blades. The lift and drag coefficients, in turn, depend upon the blade angle of attack, which is found from the relative magnitudes of the upstream flow velocity and the turbine rotational speed. The lift and drag coefficients will also be strongly dependent on the flow Reynolds number. One way to include these effects would be via empirical models for the effect of different flow parameters on turbine performance based on available data from numerical simulations or experimental results.

For the sake of brevity, other effects neglected in the present model are flow acceleration and drag from the support structures. The flow acceleration term arises from the time dependence of the tides and is included in Garrett & Cummins (2005). We have assumed that the time scale of the variation of the tide is much larger than the time it takes the flow to pass through the channel. Consequently, a quasi-steady approximation is valid. This time acceleration term could be added to the momentum equations (2.3) and (2.5), where it would have the same effect as channel bottom friction. Including it would, therefore, not lead to a qualitative change in the results presented in this paper. It should be noted, however, that unlike Vennell (2016), we do not consider the maximisation of tidal energy generation over a tidal cycle, where the variation in tidal head with time should be considered. The drag from support structures also increases the friction in channel, similar to the flow acceleration explained above. This term can cause significant power loss in channels with several rows of turbines as shown in Vennell (2012).

Lastly, we have not considered the optimisation of an array with several rows of turbines placed downstream of one another. This is partially done in Draper & Nishino (2013), who show the complexity of this issue as many combinations of row arrangement are possible. This shows the significance of an automated way of optimising turbine arrangement, such as the method of Funke *et al.* (2014), in place of manual methods for arranging the turbines.

5. Conclusions

A major challenge to the commercial extraction of tidal energy is the cost of power generation. One of the ways to bring the cost down is to optimise tidal arrays for

https://doi.org/10.1017/jfm.2017.399 Published online by Cambridge University Press

maximum power extraction per turbine. There are several factors which affect the power extraction of turbines in an array. Some of the key factors are: inherent friction in the channel, the resistance of turbines, the intra-turbine spacing in the array, the number of rows of turbines and the wake mixing caused by turbulence and swirl. There are several models in the literature that account for one or more of those key factors and show their influence on the performance of tidal arrays. However, different effects are typically considered in isolation.

In this paper, we have developed an analytical model that simultaneously considers the effects of (i) the local blockage, (ii) the free surface deformation and (iii) the added drag due to the tidal array. We show that exploring the effect of local blockage (by adjusting B_l) can significantly increase the power extraction per turbine. We find that the surface deformation effect, which is higher at higher Froude numbers, leads to the requirement of slightly higher turbine resistance and slightly more closely packed turbines to achieve the maximum possible power extraction per turbine. We find that the effect of added drag, which is higher in channels with smaller inherent drag coefficient (C_f), partially or completely nullifies the supposed advantage of increasing the global blockage B_g. The effect of added drag is found to be crucial in determining the turbine resistance required to achieve maximum C_{PG} and also reduces the optimal local blockage (B_l^{opt}) slightly. In very short channels with very high seabed friction coefficient, the effect of the friction at the array scale is also found to be important. It increases the optimal local blockage and decreases the optimal turbine resistance noticeably.

Most importantly, we find that the effects of local blockage and added drag must be considered simultaneously in order to determine the optimal channel blockage and the required turbine resistance for a tidal array with maximum power extraction per turbine. In isolation, both effects will lead to over-estimates of both the global blockage and the turbine resistance required for optimum array design. We, therefore, conclude that considering one of the two effects alone will lead to the addition of unnecessary turbines and the higher wastage of power through dissipation.

Finally, the importance has been shown of including all the factors that affect the power extraction of an array in one model. This is because the optimal design is a result of an interplay between different effects. The present model includes three important effects: the local blockage, the added drag due to the tidal array and the surface deformation. In future, the influence of other factors, such as the flow Reynolds number, turbulence intensity, velocity and density profiles as well as the swirling flow imparted by the turbines, should be analysed and those factors that are found to be important should be incorporated along with the three factors already present in the model here.

Acknowledgements

The authors wish to thank R. Willden, T. Nishino, C. Vogel and others for the very helpful discussions at the Oxford Tidal Energy workshop. The work was mainly funded by the Newton Fund through EPSRC, UK (EP/M019896/1). The first author was supported by NSFC, China (grant no. 11672123) during the later stages of this research.

Appendix A. Final set of equations

The final set of 12 equations are given below in terms of 12 unknown variables (U_{1nd}, C_{TG}, α_c, α_{2A}, α_{4A}, β_{4A}, H_4, α_{2L}, α_{4L}, β_{4L}, m_1k_1 and m_4k_4), five design parameters

https://doi.org/10.1017/jfm.2017.399 Published online by Cambridge University Press

(B_g, B_a, B_l, n and a) and three channel parameters (C_f, L_c and Fr). These equations are numerically solved in Python using a Newton–Raphson method.

$$\alpha_c B_a + 0.5(\beta_{4A} + 1)(1 - B_a) = 1, \tag{A 1}$$

$$U_{1nd}^2 = \frac{C_f}{C_f + C_{fm}} - \frac{C_{TG} B_g}{C_f + C_{fm}}, \tag{A 2}$$

$$\beta_{4A}\left(H_4 - B_a \frac{\alpha_{2A}}{\alpha_{4A}}\right) = 1 - \alpha_{2A} B_a, \tag{A 3}$$

$$B_l C_{TG} = U_{1nd}^2(\beta_{4A}^2 - \alpha_{4A}^2), \tag{A 4}$$

$$H_4 = 1 - \frac{Fr^2}{2} U_{1nd}^2[(\beta_{4A}^2 - 1) + C_{fm2}], \tag{A 5}$$

$$2U_{1nd}^2[1 - \beta_{4A} + \alpha_{2A} B_a(\beta_{4A} - \alpha_{4A})] = C_{TG} B_g + U_{1nd}^2 C_{fm2} - \frac{1}{Fr^2}(1 - H_4^2), \tag{A 6}$$

$$\beta_{4L} = \frac{1 - \alpha_{2L} B_l}{1 - \dfrac{\alpha_{2L}}{\alpha_{4L}} B_l}, \tag{A 7}$$

$$C_{TG} = U_{1nd}^2 \alpha_{2A}^2 (m_4 k_4)^2 [\beta_{4L}^2 - \alpha_{4L}^2], \tag{A 8}$$

$$\begin{aligned} \frac{(m_4 k_4)^2}{2}(\beta_{4L}^2 - \alpha_{4L}^2) \;=\; & \frac{m_1 k_1}{B_l} - m_4 k_4 \alpha_{4L} \alpha_{2L} - \frac{m_4 k_4 \beta_{4L}^2}{B_l} + m_4 k_4 \beta_{4L}^2 \frac{\alpha_{2L}}{\alpha_{4L}} \\ & + \frac{1}{2 B_l m_4 k_4}[(m_4 k_4 \beta_{4L})^2 - (m_1 k_1)^2], \end{aligned} \tag{A 9}$$

$$\alpha_{2L} = m_1 k_1 (1 - a), \tag{A 10}$$

$$m_1 k_1 = \left[1 + \left(\frac{1}{n}\right)(\alpha_{2A} - 1)\right]^{-1}, \tag{A 11}$$

$$m_4 k_4 = \left[1 + \left(\frac{1}{n}\right)\left(\frac{\alpha_{2A}}{\alpha_{4A}} - 1\right)\right]^{-1}. \tag{A 12}$$

Where $C_{fm} = (2 f_1 L_{15A}/h_1)(B_a \alpha_c^2 + (1 - B_a)((1 + \beta_{4A})/2)^2 - 1)$ and $C_{fm2} = (2 f_1 L_{14A}/h_1)(B_a \alpha_c^2 + (1 - B_a)((1 + \beta_{4A})/2)^2)$ are friction terms due to the array-induced axial flow speed variations and drag at the array scale, respectively.

The length parameters are $L_{14A} = 0.7 L_{15A}$ and $L_{15A} = L_{Array}(((n - 1)B_l + 1)/n)$ and L_{Array} is linearly proportional to B_g in a given channel.

REFERENCES

ADCOCK, T. A., DRAPER, S. & NISHINO, T. 2015 Tidal power generation – a review of hydrodynamic modelling. *Proc. Inst. Mech. Engrs* A **0**, 1–17.

BETZ, A. 1920 The maximum of the theoretically possible exploitation of wind by means of a wind motor. *Wind Engng* **37** (4), 441–446.

BRYDEN, I. G. & COUCH, S. J. 2007 How much energy can be extracted from moving water with a free surface: a question of importance in the field of tidal current energy? *J. Renew. Energy* **32** (11), 1961–1966.

DIVETT, T., VENNELL, R. & STEVENS, C. 2011 Optimisation of multiple turbine arrays in a channel with tidally reversing flow by numerical modelling with adaptive mesh. *Phil. Trans. R. Soc.* A **371**, 20120251.

https://doi.org/10.1017/jfm.2017.399 Published online by Cambridge University Press

DRAPER, S., HOULSBY, G. T., OLDFIELD, M. L. G. & BORTHWICK, A. G. L. 2010 Modelling tidal energy extraction in a depth-averaged coastal domain. *IET Renew. Power Gener.* **4** (6), 545–554.

DRAPER, S. & NISHINO, T. 2013 Centred and staggered arrangements of tidal turbines. *J. Fluid Mech.* **739**, 72–93.

FUNKE, S. W., FARRELL, P. E. & PIGGOTT, M. D. 2014 Tidal turbine array optimisation using the adjoint approach. *J. Renew. Energy* **63**, 658–673.

GARRETT, C. & CUMMINS, P. 2005 The power potential of tidal currents in channels. *Proc. R. Soc. Lond.* A **461** (2060), 2563–2572.

GARRETT, C. & CUMMINS, P. 2007 The efficiency of a turbine in a tidal channel. *J. Fluid Mech.* **588**, 243–251.

GARRETT, C. & CUMMINS, P. 2013 Maximum power from a turbine farm in shallow water. *J. Fluid Mech.* **714**, 634–643.

LANCHESTER, F. W. 1915 A contribution to the theory of propulsion and the screw propeller. *Trans. Inst. Nav. Arch.* **57**, 98–116.

MEHTA, D., VAN ZUIJLEN, A. H., KOREN, B., HOLIERHOEK, J. G. & BIJL, H. 2014 Large eddy simulation of wind farm aerodynamics: a review. *J. Wind Engng Ind. Aerodyn.* **133**, 1–17.

NISHINO, T. & WILLDEN, R. H. J. 2012*a* Effects of 3-D channel blockage and turbulent wake mixing on the limit of power extraction by tidal turbines. *Intl J. Heat Fluid Flow* **37**, 123–135.

NISHINO, T. & WILLDEN, R. H. J. 2012*b* The efficiency of an array of tidal turbines partially blocking a wide channel. *J. Fluid Mech.* **708**, 596–606.

NISHINO, T. & WILLDEN, R. H. J. 2013 Two-scale dynamics of flow past a partial cross-stream array of tidal turbines. *J. Fluid Mech.* **730**, 220–244.

PORTÉ-AGEL, F., WU, Y., LU, H. & CONZEMIUS, R. J. 2011 Large-eddy simulation of atmospheric boundary layer flow through wind turbines and wind farms. *J. Wind Engng Ind. Aerodyn.* **99** (4), 154–168.

VENNELL, R. 2010 Tuning turbines in a tidal channel. *J. Fluid Mech.* **663**, 253–267.

VENNELL, R. 2011 Tuning tidal turbines in-concert to maximise farm efficiency. *J. Fluid Mech.* **671**, 587–604.

VENNELL, R. 2012 The energetics of large tidal turbine arrays. *J. Renew. Energy* **48**, 210–219.

VENNELL, R. 2016 An optimal tuning strategy for tidal turbines. *Proc. R. Soc. Lond.* A **472** (2195), 20160047.

VENNELL, R., FUNKE, S. W., DRAPER, S., STEVENS, C. & DIVETT, T. 2015 Designing large arrays of tidal turbines: a synthesis and review. *Renew. Sustain. Energy Rev.* **41**, 454–472.

VOGEL, C. R., HOULSBY, G. T. & WILLDEN, R. H. J. 2016 Effect of free surface deformation on the extractable power of a finite width turbine array. *J. Renew. Energy* **88**, 317–324.

WHELAN, J. I., GRAHAM, J. M. R. & PEIRÓ, J. 2009 A free-surface and blockage correction for tidal turbines. *J. Fluid Mech.* **624**, 281–291.

https://doi.org/10.1017/jfm.2017.399 Published online by Cambridge University Press